ChemPubSoc Europe

DOI: 10.1002/chem.201900718

CHEMISTRY A European Journal Full Paper

Photodynamic Therapy

Hitherto-Unexplored Photodynamic Therapy of Ag_2S and Enhanced Regulation Based on Polydopamine In Vitro and Vivo

Kai Cheng,[a] Xiao-Shuai Zhang,[a] Jie An,[a] Cheng Li,[a] Ruo-Yun Zhang,[a] Run Ye,[c] Bang-Jiao Ye,[c] Bo Liu,[a] and Yuan-Di Zhao*[a, b]

Abstract: Given their superior penetration depths, photosensitizers with longer absorption wavelengths present broader application prospects in photodynamic therapy (PDT). Herein, Ag_2S quantum dots were discovered, for the first time, to be capable of killing tumor cells through the photodynamic route by near-infrared light irradiation, which means relatively less excitation of the probe compared with traditional photosensitizers absorbing short wavelengths. On modification with polydopamine (PDA), PDA-Ag_2S was obtained, which showed outstanding capacity for inducing reactive oxygen species (increased by 1.69 times). With the addition of PDA, Ag_2S had more opportunities to react with surrounding O_2, which was demonstrated by typical triplet electron spin resonance (ESR) analysis. Furthermore, the PDT effects of Ag_2S and PDA-Ag_2S achieved at longer wavelengths were almost identical to the effects produced at 660 nm, which was proved by studies in vitro. PDA-Ag_2S showed distinctly better therapeutic effects than Ag_2S in experiments in vivo, which further validated the enhanced regulatory effect of PDA. Altogether, a new photosensitizer with longer absorption wavelength was developed by using the hitherto-unexplored photodynamic function of Ag_2S quantum dots, which extended and enhanced the regulatory effect originating from PDA.

Introduction

Cancer is one of the primary threats to human health, hence methods for cancer diagnosis and treatment are widely needed. In recent years, photodynamic therapy (PDT), a non-invasive treatment method, has been rapidly developed in the field of cancer treatment, making it one of the most appealing research fields in cancer prevention.[1–3] The basic principle of PDT is that the photosensitizer is first excited from the ground state by absorbing visible or near infrared (NIR) light energy, and subsequently reacts with surrounding oxygen molecules to produce highly active and toxic photochemical products, such as reactive oxygen species (ROS),[4] etc. These substances can directly induce apoptosis or necrosis, or destroy blood vessels in tumor stroma, leading to tumor ischemia and hypoxia, and also initiate specific immune mechanisms to enhance antitumor effects.

The light source and photosensitizer play decisive roles in PDT and are constantly being updated owing to insistent clinical demands. For the light source, the emergence of miniaturized semiconductor lasers[5] overcame the shortcomings of early ruby lasers, which were bulky and lacked stability,[6] thus meaning the limitations of the light source for PDT are basically resolved.

In general, light sources with longer wavelengths present stronger penetration into tissue. For instance, light of 600, 700, and 800 nm can penetrate tissue to depths of about 0.5, 0.8, and 1 cm, respectively.[7] Therefore, with the increase of wavelength within the optical window of the human body, the therapeutic range of PDT is also broader. For the photosensitizer, the second-generation porphyrin-based photosensitizer is widely used for the sake of its shorter photoactive period,[8] longer absorption wavelength,[9] and lower phototoxicity for skin compared with the first-generation photosensitizer. However, disadvantages still exist concerning the low target efficiency in cells and the relatively short wavelength, which does not satisfy the need for deeper treatment depth;[10] these have adversely affected its further clinical application. Hence, exploring photosensitizers with longer absorption wavelengths for deeper treatment depth is of significance for the application of PDT.

[a] K. Cheng, X.-S. Zhang, J. An, C. Li, R.-Y. Zhang, Prof. Dr. B. Liu, Prof. Dr. Y.-D. Zhao
Britton Chance Center for Biomedical Photonics
at Wuhan National Laboratory for Optoelectronics
Hubei Bioinformatics & Molecular Imaging Key Laboratory
Department of Biomedical Engineering
College of Life Science and Technology
Huazhong University of Science and Technology
Wuhan 430074, Hubei (P. R. China)
E-mail: zydi@mail.hust.edu.cn

[b] Prof. Dr. Y.-D. Zhao
Key Laboratory of Biomedical Photonics (HUST), Ministry of Education
Huazhong University of Science and Technology
Wuhan 430074, Hubei (P. R. China)

[c] R. Ye, Prof. Dr. B.-J. Ye
State Key Laboratory of Particle Detection and Electronics
University of Science and Technology of China
Hefei 230026 (P. R. China)

Supporting information and the ORCID identification number(s) for the author(s) of this article can be found under: https://doi.org/10.1002/chem.201900718.

The development of nanotechnology, especially in terms of the urgent demands for PDT, has facilitated the frequent emergence and application of nanomaterials in the field of biomedicine. Quantum dots (QDs), a type of well-known nanomaterial, have achieved great success in the biomedical field owing to their excellent optical properties. As has been demonstrated, the latest low-toxicity Ag_2S QDs can realize a wide range of wavelength absorption with the fluorescence emission reaching the NIR II region (1000–1300 nm), making them of practical value for in vivo fluorescence imaging.[11–13] Current research has demonstrated that Ag_2S QDs also possess photothermal effects,[12,13] making them a valuable multifunctional nanomaterial. Nevertheless, to the best of our knowledge, no research on the photodynamic behavior of Ag_2S has been reported, and we are excited to report here the noteworthy photodynamic behavior of Ag_2S.

In this paper, Ag_2S QDs were first synthesized by high temperature pyrolysis. After modification with PEGylated phospholipids, the nanoparticles were found to be capable of inducing singlet oxygen ($^1O_2$) production and killing tumor cells under the irradiation of 808 nm NIR. After further coupling of the nanoparticles to the surface of polydopamine (PDA), more ROS could be produced with the regulation of PDA, endowing the Ag_2S-PDA with stronger PDT effects. This work extends the application of the photodynamic therapeutic functions of Ag_2S, and provides a new route for the development of photosensitizers with longer absorption wavelengths, avoiding the unwanted phototoxicity.

Results and Discussion

In this paper, two steps were taken to obtain the PDA-Ag_2S including the synthesis of PDA through self-polymerization of dopamine and addition of the polyethylene glycol (PEG)-wrapped Ag_2S QDs onto PDA (Figure 1).[14–17] After the process, a series of characterization tests for the coupling process was carried out. Electron microscopy made it clear that the PDA and Ag_2S were uniformly dispersed, PDA was determined to be about 90 nm (Figure 2A and B) with the size of Ag_2S was about 2–5 nm (Figure 2D). High-resolution (HR)TEM images (Figure S1A and B in the Supporting Information) show that the silver sulfide quantum dots had good crystal structure and

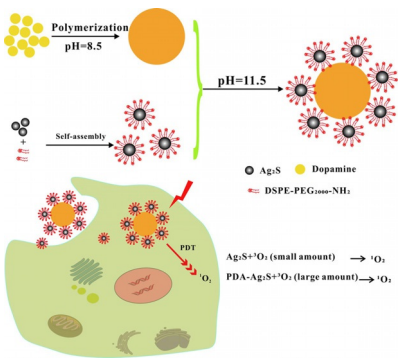

Figure 1. Synthesis of the probe and its photodynamic mechanism.

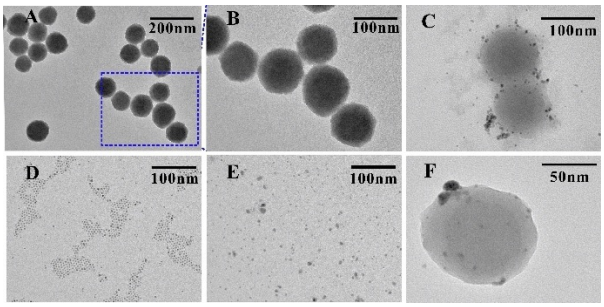

Figure 2. TEM of PDA (A, B: enlarged), PDA-Ag_2S (C and F), Ag_2S (D), and A-NH_2 (E).

prominent lattices. Meanwhile, the diffraction (Figure S1C in the Supporting Information) was also good proof for the crystal structure of silver sulfide quantum dots. After modification of silver sulfide with DSPE-PEG_{2000}-NH_2 (Figure 2E and Figure S2 in the Supporting Information), it was found that the Ag_2S-DSPE-PEG_{2000}-NH_2 (A-NH_2) wrapped single nanoparticles were dominant. When A-NH_2 was attached to the PDA surface, it was observed that A-NH_2 was primarily immobilized on the PDA spherical surface (Figure 2C and F), but there still existed a small amount of free A-NH_2, so from here-on PDA-Ag_2S refers to the mixture of free A-NH_2 and PDA-Ag_2S. Dynamic light scattering (DLS) results showed that the particle size distribution of PDA shifted by about 20 nm after modification with A-NH_2 (Figure S3A in the Supporting Information), meanwhile, the zeta potential also changed from −43.10 to −21.80 mV (Figure S3B in the Supporting Information), implying a significant influence of the positively charged amino group of A-NH_2. All of the above evidence demonstrated that we have successful synthesized PDA-Ag_2S nanoparticles. In addition, we did not notice significant changes to the absorption before and after the immobilization of A-NH_2 to the PDA, and the characteristic small absorption peak in the absorption spectrum of PDA-Ag_2S was consistent with PDA at 280 nm (Figure 3A), and the absorption in the NIR region was almost unchanged after modification. Furthermore, the IR spectrum revealed the characteristic peaks of the C=C skeleton in the benzene ring at 1600 cm^{-1}, which were found both in PDA and PDA-Ag_2S, in addition to the stretching vibration of aromatic hydrogen at 3000–3200 cm^{-1} (Figure S4 in the Supporting Information). In addition, the stretching vibration of saturated C–H at 2800–3000 cm^{-1} was observed for PDA-Ag_2S and A-NH_2. All these results demonstrated that PEG-wrapped Ag_2S was conjugated to PDA, accompanied with a certain extent of physical adsorption.

Next, the photodynamic behavior of the probe was determined. 1,3-Diphenylisobenzofuran (DPBF) is one of the most active singlet oxygen detectors. Singlet oxygen can attack the furan ring in the DPBF structure to make it open, which results in the change of DPBF absorption at 410 nm, so it is usually chosen as an indicator of singlet oxygen. In our experiments, the probe was incubated with DPBF and the absorption spectrum was measured after laser irradiation. The results showed that the absorption peak of DPBF at 410 nm decreased with

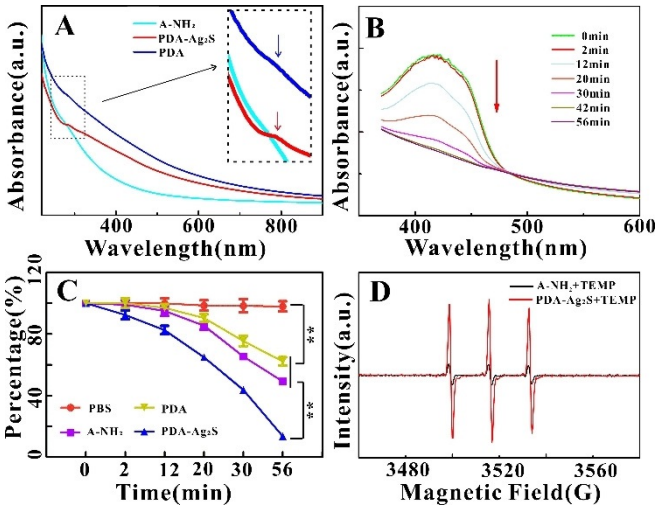

Figure 3. Absorption spectra of A-NH_2, PDA, and PDA-Ag_2S (A). Absorption spectra of DPBF incubated with PDA-Ag_2S after different laser irradiation times (B). The change at 410 nm of PBS, PDA, A-NH_2, and PDA-Ag_2S after different laser irradiation times (C). ESR spectra after A-NH_2 and PDA-Ag_2S mixed with TEMP irradiated with an 808 nm laser for 10 min (D).

prolonged laser irradiation time and nearly disappeared after 42 min, indicating that the furan ring was significantly depleted by the probe through the production of $^1O_2$ after irradiation, thus causing the DPBF absorption at 410 nm to reduce (Figure 3B). Comparing the effects of the different materials on DPBF absorption at 410 nm (Figure 3C), both PDA and Ag_2S had significantly stronger $^1O_2$ production capacity than phosphate buffered saline (PBS; $p < 0.01$), and PDA-Ag_2S had greater $^1O_2$ production capacity than the PDA and Ag_2S alone ($p < 0.01$), which was 1.73 times than that of the Ag_2S group alone regarding DPBF absorption change at 410 nm, suggesting that the introduction of PDA significantly enhanced the $^1O_2$ production capacity, which gives a sound foundation for the subsequent PDT application of the probe. Meanwhile, the effects of free A-NH_2 on PDA-Ag_2S were investigated (Figure S5 in the Supporting Information). It was clear that the reactive oxygen species inducing ability of the free A-NH_2 (not connected to PDA) was significantly lower than that of PDA-Ag_2S, which further demonstrated the distinct reactive oxygen species inducing activity of PDA-Ag_2S. We also rated the singlet oxygen generation efficiency of our probe and the prevalently used photosensitizers such as Ce6 (Figure S6 in the Supporting Information). The singlet oxygen generation efficiency of Ce6 was the highest, although our probe has the advantage of using near-infrared light to stimulate it, which can be more suitable for high-depth treatment in vivo. Furthermore, $^1O_2$ production was measured by ESR. Owing to the short lifetime of singlet oxygen, 2,2,6,6-tetramethylpiperidine (TEMP) is often used as the $^1O_2$ capture agent.[18] It was found that the typical signals of $^1O_2$[19] were detected with the A-NH_2 group under 808 nm laser treatment by triple ESR, which indicated that A-NH_2 was effective at generating $^1O_2$ after laser induction, and in the meanwhile, a stronger ESR triplet signal could be seen for the PDA-Ag_2S group, demonstrating that PDA-Ag_2S had higher $^1O_2$ production capacity (Figure 3D). We also investigated the regulation of PDA on Ag_2S with positron annihilation lifetime spectra (PALS). From the measurement results (Figure S7 and Table S1 in the Supporting Information), there were two lifetime components owing to defects in silver sulfide. Here, the short component $\tau_1 = (250.1 \pm 3.1)$ ps represents annihilation in the vacancies of the metallic sublattices of Ag_2S, and the longer component $\tau_2 = (403.4 \pm 17.0)$ ps corresponds to the annihilation in the defects at interfaces. After modification with polydopamine, three types of annihilation sites in PDA-Ag_2S were found. That was, there were three lifetime components, τ_1 (275.2 ± 13.0 ps), τ_2 (401.3 ± 27.1 ps), and τ_3 (1986.1 ± 50.0 ps). Notably, τ_1 (275.2 ± 13.0 ps) and τ_2 (401.3 ± 27.1 ps) matched the lifetimes of A-NH2, whereas the long-lived τ_3 (1986.1 ± 50.0 ps) in PDA-Ag_2S was ascribed to polydopamine, implying that part of the positrons annihilate in the pores of polydopamine, which yielded a longer lifetime component owing to the modification of polydopamine, which demonstrated that a greater specific surface area of silver sulfide was obtained when silver sulfide was modified on the surface of PDA.

Cell experiments are a prerequisite for in vivo application of the probe. Therefore, MTT assays of the A-NH_2 and PDA-Ag_2S were performed to investigate their cytotoxicity. As a result, after incubating A-NH_2 (0–400 μg mL^{-1}) and PDA-Ag_2S (0–400 μg mL^{-1}) with HeLa, MCF-7, and 4T1 cells for 24 h, survival rates of the three cells were as high as 80.41, 83.45, and 82.74%, respectively, even when the concentration of A-NH_2 was 100 μg mL^{-1} (Figure 4A), and those of PDA-Ag_2S groups can reach 79.53, 83.32, and 80.32% (Figure 4B), hinting that A-NH_2 and PDA-Ag_2S were both of good biocompatibility and low cytotoxicity, which thus guaranteed the safety for cell PDT.

Similarly, through the standard MTT assay, the photodynamic killing effect of A-NH_2 and PDA-Ag_2S (40 μg mL^{-1} Ag_2S and 80 μg mL^{-1} PDA) on three tumor cell lines were also examined. To study the influence of laser wavelength on the probes, the commonly used 660 nm and 808 nm lasers were selected. Results showed that the survival rates of the three groups were

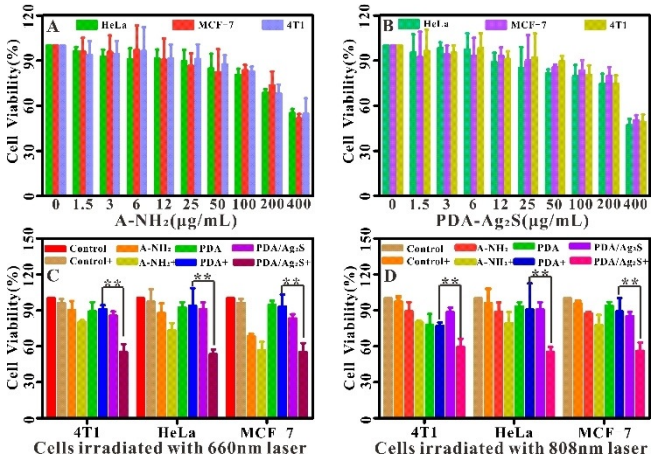

Figure 4. MTT results of HeLa, MCF-7, and 4T1 cells incubated with different concentrations of A-NH_2 (A) and PDA-Ag_2S (B). Cell viability of different probes (40 μg mL^{-1} Ag_2S, 80 μg mL^{-1} PDA) incubated with three cell lines after irradiation with a 660 nm (C) or 808 nm (D) laser.

96.3, 97.14, and 96.25% after 660 nm laser irradiation (Figure 4C), and the 808 nm laser groups were 97.34, 96.35, and 95.61%, respectively (Figure 4D), indicating that the laser itself did not affect the survival of cells. After 660 nm laser irradiation, the survival rates of the three cell lines treated with A-NH_2 decreased by 9.78, 14.43, and 11.82%, the PDA-treated cells only decreased by −1.89, 1.34, and 1.71%, whereas PDA-Ag_2S-treated cells decreased by 30.1, 37.35, and 28.06%, respectively (Figure 4C). By comparison of these data, it was clear that A-NH_2 had significant PDT effect, the reason was presumably that the electrons of Ag_2S were converted to the excited state under laser irradiation, and it had a certain probability to reach the triplet excited state, which remains for milliseconds, providing sufficient time for the reaction between Ag_2S and oxygen molecules, releasing energy and returning to the ground state.[20] At the same time, oxygen molecules in the ground state got energy from Ag_2S, and generated $^1O_2$ with high chemical activity, which had a good killing effect on cells. The viability of PDA-Ag_2S treatment was significantly lower than that of A-NH_2 or PDA alone, which was possibly due to the production of partial $^1O_2$ resulting from Ag_2S after laser irradiation. However, because of the defects on the surface of the QDs, some of the excited electrons fell into the trapping state of the QDs and could not return to the holes,[20] whereas the polyphenols on the surface of PDA were easily oxidized, the electrons of which were transferred to the empty spaces of the QDs, promoting the formation of the excited state of the Ag_2S triplet state. Meanwhile, PDA itself was oxidized to quinone, which further reacted with oxygen to form active superoxide ions, then the superoxide ions continued to generate HO_2 and $^1O_2$ to produce stronger PDT effects.

After 808 nm laser irradiation, the survival rates of the three cells were reduced to 8.78, 9.43, and 9.82% under A-NH_2 treatment, whereas those for the PDA groups were 1.12, 2.66, and 4.71%, and the PDA-Ag_2S groups were 29.12, 35.35, and 29.08%, respectively (Figure 4D). It was clear that the cell killing effects of the 808 nm laser was similar to those of the 660 nm laser, which was likely due to the small absorption difference of the probe between 660 and 808 nm. Meanwhile, it also showed that PDT could be achieved at the longer 808 nm wavelength and the effect was basically identical to that of 660 nm for A-NH_2 and PDA-Ag_2S.

These studies confirmed that both Ag_2S and PDA have photothermal conversion capability.[12,21] Therefore, to further verify whether the cell death was derived from the photothermal or PDT effect, the effect of temperature resulting from the photothermal effect on cell survival rate was investigated. In this experiment, photothermal analysis was performed by using probes at the same concentration as in the cell experiment. Experiments showed that the maximum temperature of PDA-Ag_2S at this concentration reached about 36 °C after 10 min irradiation (Figure S8 in the Supporting Information), so the effect of temperature on cell viability was simulated at a higher temperature of 40 °C. Results showed that survival rates of the three cell lines treated with A-NH_2 at 40 °C were 16.67, 16.02, and 14.83% higher than their irradiation groups, the PDA groups were 6.94, −1.37, and 3.23% higher than their irradiation groups, and the PDA-Ag_2S groups were 35.55, 38.49, and 36.19% higher than their irradiation groups, respectively (Figure S9 in the Supporting Information). These results were sufficient to confirm that the photothermal effect on cell viability was negligible at this concentration. Therefore, the death of the probe-treated cells after laser irradiation was indeed caused by the PDT effect.

To verify the photodynamic behavior of A-NH_2 and PDA-Ag_2S under long wavelength excitation, the 2,7-dichlorodihydrofluorescein (DCFH-DA) reactive oxygen fluorescence detection kit was used to detect the active oxygen status in cells treated with different methods. In our results, after 808 nm laser irradiation, blank cells displayed a fluorescence peak at 525 nm (Figure S10A in the Supporting Information), implying that the cells contained a certain amount of ROS at this time, whereas the fluorescence peak of cells incubated with PDA increased to some extent, which was probably due to the oxidization of polyphenols on PDA, changing the surrounding oxygen molecules into charged radicals by redox reaction, and eventually causing the generation of active oxygen. The fluorescence peak of cells incubated with A-NH_2 was significantly enhanced, manifesting that Ag_2S induced more reactive oxygen species after laser irradiation, whereas the PDA-Ag_2S group enhancement was again more significant, demonstrating that PDA-Ag_2S had the highest ability to induce the production of reactive oxygen species. Moreover, the enhancement of fluorescence intensity was significantly different from that of the PDA group and A-NH_2 group ($p < 0.001$), and the changed value of fluorescence intensity was 1.69 times stronger than the equivalent concentration of A-NH_2. Further observation could also demonstrate that the increase in fluorescence intensity of the PDA-Ag_2S group was higher than the sum of enhancements in PDA group and Ag_2S group, proving that PDA significantly enhanced the probe's capacity for active oxygen production after A-NH_2 was modified onto it, which was consistent with results of Figure 4. This conclusion was also confirmed by fluorescence imaging experiments (Figure 5A), which showed that the intracellular fluorescence on PDA-Ag_2S treatment was significantly stronger than the other three groups. For 660 nm-laser-treated cells, the results were similar to those of 808 nm laser treatment (Figure 5B and Figure S10B in the Supporting Information), indicating that for A-NH_2 and PDA-Ag_2S, the production of ROS could be performed at this longer wavelength and achieved the same effect as 660 nm, which was in accord with the MTT results (Figure 4C and D). From Figure 3A, it is clear that the absorption of the probe was gradually diminished as the wavelength increased, which is the reason we used 808 and 660 nm lasers to explore the different effects between near-infrared and visible light laser excitation. The probes were incubated with HeLa, MCF-7, and 4T1 cells. After 660 nm laser irradiation, the survival rates of the three cell lines treated with PDA-Ag_2S decreased by 30.1, 37.35, and 28.06%, respectively (Figure 4C). After 808 nm laser irradiation, the survival rates of the three cells were reduced to 29.12, 35.35, and 29.08% under PDA-Ag_2S treatment, respectively (Figure 4D). The cytotoxic effects of the two laser treatments were similar; the effect produced by the 808 nm

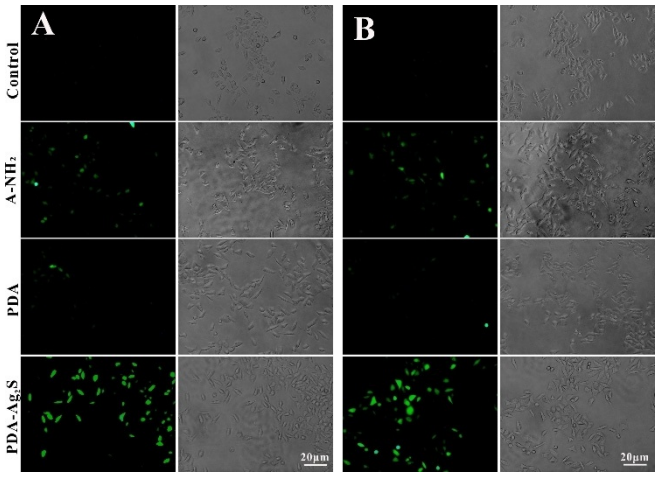

Figure 5. Corresponding local fluorescence images of DCFH-DA staining after incubation with different probes and HeLa cells for 4 h and then irradiated with an 808 nm (A) or 660 nm (B) laser for 10 min.

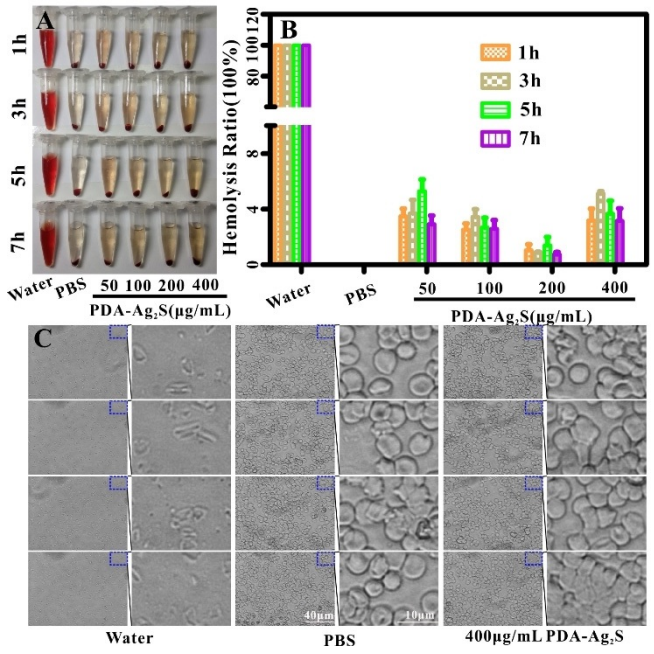

Figure 6. The white light (A) and hemolytic rate (B) of the supernatant after incubation of red blood cells (RBC) with different concentrations of the probe. Micrograph and local enlargement of the cell smear made by cell precipitation (C).

laser was not worse than the 660 nm laser. We conducted the penetration depth test by using a self-built detection device (Figure S11 B and C in the Supporting Information) to authentically reflect the penetration depth. The results showed that the 808 nm laser had a stronger penetration depth than the 660 nm laser under the same power (Figure S11 A in the Supporting Information). In addition, the deeper penetration depth of the 808 nm laser will make treatment more thorough and effective.

As blood compatibility of a probe is an important part of the biosafety evaluation, hemolysis tests of the probe were investigated by co-incubating the probe with red blood cells (RBC). Results showed that the hemolysis rate of RBC was 100% in ultra-pure water and none in PBS (Figure 6 A and B), which was caused by different osmotic pressures. Almost all of the RBC sank, and the supernatant (Figure S12 in the Supporting Information) changed monotonously after addition of RBC when the system contained the probe (Figure 6 A). Even when the probe concentration was as high as 400 $\mu g\,mL^{-1}$, the hemolysis rate was still low after 7 h of incubation (Figure 6 C), and the red blood cells were in a good state (Figure 6 C) although fragmentation was observed in pure water, reflecting that probe had good compatibility with blood and a mild influence on RBC, which guaranteed the safety of the follow-up tests in vivo.

Encouraged by the promising results obtained above, we further assessed the in vivo therapeutic effect of the probes on 4T1 tumor bearing female mice. To judge whether there is an influence coming from the photothermal effect, temperature changes were recorded with time. The temperature change in the PDA-Ag_2S group was nearly consistent with the PBS group (Figure S13 in the Supporting Information), indicating the impact of the photothermal heating was negligible, so we could definitely say that the therapeutic effect was not produced by photothermal heating after irradiation with the laser. The size of the tumor was measured to assess the therapeutic effect after intratumor injection of the probes (Figure 7 B and C). It was found that the treatment could be divided into three categories. i) The changes of tumors in mice treated with PBS, PDA-Ag_2S, and laser irradiation alone were similar, and the tumor volume increased over time, indicating that Ag_2S and PDA without laser irradiation, and laser alone had no therapeutic effect on the tumor. ii) Tumor growth in the A-NH_2 groups was slower and the volume was notably smaller than that of category (i), and there was a very significant difference between the two categories ($p < 0.01$; Figure 7 B, C, and D). In addition, the tumors disappeared in the first 12 d, followed by two mice displaying reappearing tumors among the first two groups (Figure 7 C and D). iii) For the PDA-Ag_2S group, no recurrence was found during statistical time, which was extremely different from the other categories ($p < 0.01$), suggesting that the PDA-Ag_2S group gave the best therapeutic effect by exerting the regulation of PDT. Monitoring of the body weight of mice showed that all groups of mice decreased after 2 d, which might be due to the effect of the anesthetic drug leading to poor appetite in mice. After 4 d, the weight of the mice gradually began to increase (Figure 7 A), and the treatment groups were principally the same as those of the control group, demonstrating that the probe had no significant toxicity to mice. In addition, HE (hematoxylin and eosin) staining of organs and tumors were conducted after 6 h of treatment (Figure 7 E and Figure S14 in the Supporting Information). From this, it could be seen that the contours of the heart, liver, spleen, lung, kidney, and small intestine cells were clear in the PBS, PBS + laser, PDA-Ag_2S, A-NH_2 + laser, and PDA-Ag_2S + laser groups, and it was clear that the nuclear structure was not significantly destroyed in each group. Whereas in tumor cells, although the 4T1 cells were in good shape without large-scale

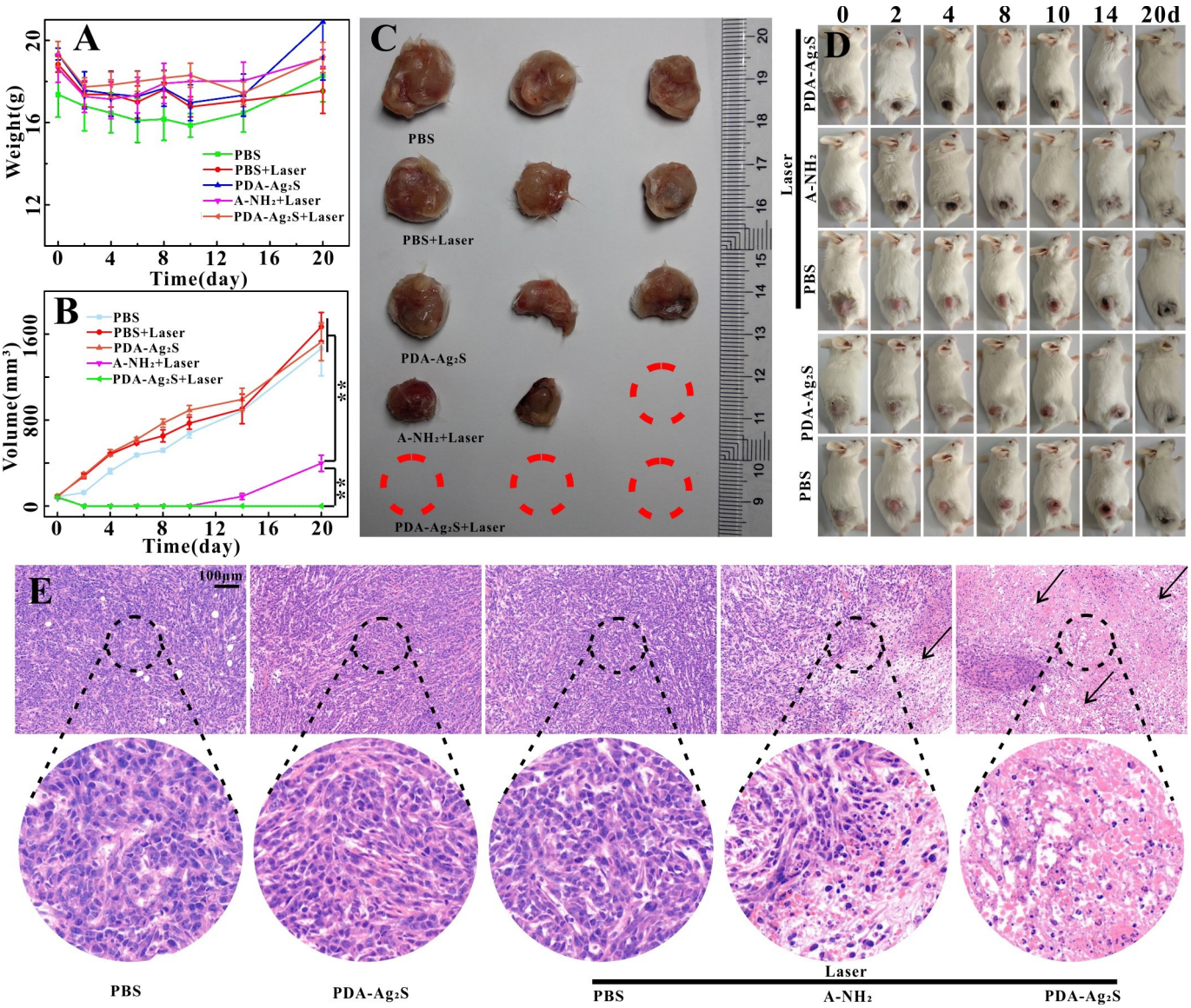

Figure 7. Tumor weight change (A), volume change (B), tumor white-light (C), white light (D) after tumor irradiation (10 min, 808 nm, 1 W cm^{-2}) in tumor-bearing mice after injection of PBS, A-NH_2, and PDA-Ag_2S, and HE staining of tumors for each group (E).

destruction in the PBS, PBS-Ag_2S, and PBS + laser groups, clear cell atrophy and nucleoplasm separation were observed in the A-NH_2 + laser and PDA-Ag_2S + laser groups, and cell damage was more serious in the latter, which also showed that PDA-Ag_2S had a better photodynamic killing effect on tumor cells than the A-NH_2 after laser group. Therefore, the characteristics of PDT regulation would make a good application prospect.

Conclusion

In this paper, biocompatible Ag_2S QDs were developed to give successful 808 nm NIR-induced photodynamic behavior. The enhanced capability of inducing $^1O_2$ was markedly regulated through PDA modification. Because longer light is capable of penetrating into deeper tissue, this photosensitizer with longer excitation wavelength has enormous implications for expanding the application of PDT to tumor therapy in vivo. Meanwhile, it is expected to contribute to the treatment of disease and improvement of health.

Experimental Section

Materials

Silver diethyldithiocarbamate (Ag(DDTC), 98%), 1-dodecanethiol (DT, 98%), *n*-hexane, acetone, and chloroform were purchased from Sinopharm Group Chemical Reagent Co., Ltd. Dopamine hydrochloride and octadecene (ODE, 90%) were purchased from Aldrich. 1,2-Distearoyl-*sn*-glycero-3-phosphoethanolamine-*N*-[methoxy(polyethylene glycol)$_{2000}$-amino (DSPE-mPEG$_{2000}$-NH_2) was purchased from Avanti. 1,3-Diphenylisobenzofuran (DPBF), thiazole blue tetrazolium bromide (MTT), and 2,2,6,6-tetramethylpiperidine (TEMP) were purchased from Aladdin. 2,7-Dichlorodihydrofluorescein diacetate (DCFH-DA) was purchased from Yi Sheng Biotechnology Co. Ltd. All reagents were of analytical grade, and used

without further purification. Four-week-old BALB/c female mice (SPF grade) were purchased from Hua Fu Kang Biotechnology Co., Ltd. All animal experiments were approved by the Animal Experimental Ethics Committee of Huazhong University of Science and Technology.

Instruments

Singlet oxygen signals were obtained with an electron spin resonance spectrometer (Bruker, Switzerland). A WFX-200 atomic absorption spectrophotometer (Beijing Beifen-Ruili Analytical Instruments Co., Ltd., China) was used to measure the concentration of Ag^+. The absorbance detection was recorded with an Elx-808 microplate reader (Biotek, USA). Purification of the probe was conducted by using a concentrator plus (Eppendorf, Germany). A QE6500 fluorescence spectrometer (Ocean Optics, USA) was used to analyze emission spectra of the probe. MDL-MD-660 nm, 2.3 W and MDL-III-808 nm, 2.5 W lasers (Changchun New Industries Optoelectronics Tech. Co., Ltd, China) were used for laser irradiation. A UV-2550 spectrophotometer (Shimadzu, Japan) was to characterize the absorption spectrum of the probe. Electron microscopy characterization was performed with a Hitachi 120 kV HT7700 transmission electron microscope (Hitachi, Japan). Particle size and zeta potential were tested by using a Nano-ZS90 nanometer (Malvern, UK).

Synthesis and concentration measurement of Ag_2S QDs

The synthesis route of Ag_2S QDs was slightly modified from a method developed by our laboratory.[22] First, Ag(DDTC) (76.8 mg) was dissolved in a mixed solution containing ODE (30 g) and DT (6 g) with Ar protection. The mixture was stirred intensely for 30 min and then heated to 100 °C and stirred 10 min to remove impurity. Then, the mixture was heated to 165 °C for 10 min, after which the solution turned from wine red to black. Finally, *n*-hexane (20 mL) was added to finish the reaction and make it cool. After that, Ag_2S QDs were purified by centrifugation with acetone (60 mL) added, the purification process was repeated three times at 12000 rpm, 10 min per time. The final stock solution was stored in chloroform at 4 °C for further use. To measure the concentration of Ag_2S, Ag_2S (2, 4, 6, 8, and 10 μL) QDs were dried by using Ar, and then dissolved in HNO_3 (100 μL, 65%, GR) for further analysis with an atomic absorption spectrophotometer.

Synthesis of PDA

According to the literature,[23] a 250 mL round-bottom flask containing ultrapure water (90 mL) was placed in oil bath to maintain the water temperature at 50 °C, followed by slow addition of dopamine hydrochloride powder (180 mg) and NaOH (760 μL, 1 mol L^{-1}) under vigorous stirring. After the solution was aged for 6 h, the color of the solution changed from colorless to pale yellow and finally turned dark brown gradually, then the solution was centrifuged at 14000 rpm for 5 min and the supernatant was discarded. Then, the precipitate was washed several times with deionized water until the supernatant become transparent. Eventually, the obtained precipitate was dissolved in deionized water and centrifuged again at 4500 rpm for 5 min with the supernatant being collected, which contained the PDA nanoparticles.

Photodynamic behavior test of the probe

A-NH_2 (2.5 mL, 15 μg mL^{-1}), PDA (80 μg mL^{-1}), or PDA-Ag_2S (15 μg mL^{-1} Ag_2S, 80 μg mL^{-1} PDA) were put in a quartz cuvette. DPBF (100 μL) was added and the UV/Vis absorption spectrum was measured after treatment with a 606 nm laser (1 W cm^{-2}) or 808 nm laser (1 W cm^{-2}) for different times (0, 2, 12, 20, 30, and 56 min). Equal amounts of A-NH_2 (15 μg mL^{-1}) and PDA-Ag_2S (15 μg mL^{-1} Ag_2S, 80 μg mL^{-1} PDA) were mixed with TEMP. Triplet signals were detected with the ESR instrument after 808 nm laser irradiation for 10 min.

Cell tests of PDT

HeLa, MCF-7, and 4T1 cells were cultured similarly to the above step. Serum-free medium (200 μL) containing different concentrations of PDA-Ag_2S (40 μg mL^{-1} Ag_2S, 80 μg mL^{-1} PDA) and A-NH_2 (40 μg mL^{-1}) were added. After 4 h, the samples were washed three times with PBS and fresh medium was added. The cells were successively irradiated with a 808 nm or 660 nm laser (1 W cm^{-2}) for 10 min, followed by incubating for 24 h. Thiazole blue (20 μL, 5 mg mL^{-1}) was added to each well with fresh serum-free medium (200 μL) already in, which was removed after another 4 h of culturing, and dimethyl sulfoxide (150 μL) was added into each hole. Finally, absorption at 490 nm was measured by using a microplate reader after slow shaking for 20 min. The cell viability was calculated with the equation (Supporting Information).

Under the same culture conditions, each 500 μL volume of A-NH_2 (40 μg mL^{-1} Ag_2S), PDA (80 μg mL^{-1}), and PDA-Ag_2S (40 μg mL^{-1} Ag_2S, 80 μg mL^{-1} PDA) was added into HeLa cells with serum-free medium already present and incubated for 6 h. After washing three times with PBS, the cells were cultured with serum-free medium (500 μL) containing DCFH-DA (10 μM) and irradiated separately with a 660 or 808 nm laser (1 W cm^{-2}) for 10 min. After further incubating for 0.5 h and subsequent washing three times with PBS to remove free DCFH-DA, a portion of cells were fixed with 2.5% glutaraldehyde for 30 min and then observed under a fluorescence microscope, the remaining cells were collected with a cell scraper, and the emission spectrum of the collected cells was measured by using a fluorescence spectrophotometer with 488 nm excitation.

Blood compatibility of PDA-Ag_2S

Fresh blood (2 mL) was obtained from five-week-old BALB/c mice and quickly transferred into an EDTA k2 anticoagulant tube. To get red blood cells (RBC), centrifugation was done at 3500 rpm for 5 min. After washing several times with PBS, the suspension solution (10 μL) of RBC was added into the PDA-Ag_2S solution at systematically varied concentrations (50, 100, 200, and 400 μg mL^{-1}) and mixed completely. Then, the mixture was incubated in 5% CO_2 atmosphere at 37 °C for 1, 3, 5, or 7 h. Next, all suspensions were photographed after centrifugation at 3500 rpm for 5 min, and then the supernatant of each tube was shifted to a 96-well plate, followed by measurement of the respective absorbance at 577 nm. Finally, precipitation of the ultra-pure water group, PBS group, and PDA-Ag_2S group (400 μg mL^{-1}) were made into cell smears, and the morphologies of the red blood cells were observed under a microscope. PBS and ultra-pure water served as the negative and positive controls. The formula for the calculation of the hemolysis rate of RBC is: hemolysis rate (%) $= (OD_{sample} - OD_{saline})/(OD_{water} - OD_{saline}) \times 100\%$

In vivo PDT

Twenty BALB/c female mice (SPF) bearing 4T1 cells were divided into five groups, the weight and tumor volume of which were recorded by using digital calipers and body weight scales. Respec-

tively, 25 μL PBS, A-NH_2, and PDA-Ag_2S (the above probes, 20 μg mL^{-1} Ag_2S, 40 μg mL^{-1} PDA) were intratumorally injected into three mice, after 10 min, three mice were taken from each group to be irradiated with a 1.0 W cm^{-2} laser for 10 min and photographed by thermal imaging. In addition, HE staining of the organs and tumors was conducted after 6 h of treatment, and changes in the body weight and tumor volume of the mice were recorded.

Acknowledgments

This work was supported by the National Key Research and Development Program of China (2017YFA0700501), the National Natural Science Foundation of China (Grant No. 81771878), and the Fundamental Research Funds for the Central Universities (HUST: 2016YXMS253, 2017KFXKJC002, 2018KFYXKJC048). We also thank the Analytical and Testing Center (HUST), the Research Core Facilities for Life Science (HUST) and the Center for Nanoscale Characterization & Devices (CNCD) at WNLO of HUST for help with measurements, and the State Key Laboratory of Particle Detection and Electronics (University of Science and Technology of China) for help with PALS.

Conflict of interest

The authors declare no conflict of interest.

Keywords: Ag_2S · enhanced regulation · photodynamic behavior · photosensitizer · polydopamine

[1] C. Gao, P. Dong, Z. Lin, X. Guo, B. P. Jiang, S. Ji, H. Liang, X. C. Shen, *Chem. Eur. J.* **2018**, *24*, 12827 – 12837.
[2] A. Sourdon, M. Gary-Bobo, M. Maynadier, M. Garcia, J. P. Majoral, A. M. Caminade, O. Mongin, M. Blanchard-Desce, *Chem. Eur. J.* **2019**, *25*, 3637 – 3649.
[3] Z. Wang, Y. Gao, M. Hussain, S. Kundu, V. Rane, M. Hayvali, E. A. Yildiz, J. Zhao, H. G. Yaglioglu, R. Das, L. Luo, J. Li, *Chem. Eur. J.* **2018**, *24*, 18663 – 18675.
[4] J. Pirillo, G. Mazzone, N. Russo, *Chem. Eur. J.* **2018**, *24*, 3512 – 3519.
[5] I. Garbayo, D. Pla, A. Morata, L. Fonseca, N. Sabaté, A. Tarancón, *Energy Environ. Sci.* **2014**, *7*, 3617 – 3629.
[6] M. H. Kiang, O. Solgaard, R. S. Muller, K. Y. Lau, *IEEE Photonics Technol. Lett.* **1996**, *8*, 1707 – 1709.
[7] A. N. Bashkatov, E. A. Genina, V. I. Kochubey, V. V. Tuchin, *J. Phys. D* **2005**, *38*, 2543 – 2555.
[8] M. O. Senge, *Photochem. Photobiol.* **2012**, *9*, 170 – 179.
[9] R. Bonnett. P. Charlesworth, B. D. Djelal, S. Foley, D. J. McGarvey, T. G. Truscott, *J. Chem. Soc. Perkin Trans. 2* **1999**, 325 – 328.
[10] C. M. Iversen, T. D. Hooker, A. T. Classen, R. J. Norby, *GCB Bioenergy* **2011**, *17*, 1130 – 1139.
[11] H. Shang, Q. Di, M. Ji, B. Bai, J. Liu, W. Chen, M. Xu, H. Rong, J. Liu, J. Zhang, *Chem. Eur. J.* **2018**, *24*, 13676 – 13680.
[12] K. Cheng, X. Yang, X. Zhang, J. Chen, J. An, Y. Song, C. Li, Y. Xuan, R. Zhang, C. Yang, X. Song, Y. Zhao, B. Liu, *Adv. Funct. Mater.* **2018**, *28*, 1803118.
[13] J. Gao, C. Wu, D. Deng, P. Wu, C. Cai, *Adv. Healthcare Mater.* **2016**, *5*, 2437 – 2449.
[14] Y. Liu, K. Ai, J. Liu, M. Deng, Y. He, L. Lu, *Adv. Mater.* **2013**, *25*, 1353 – 1359.
[15] K. Y. Ju, Y. Lee, S. Lee, S. B. Park, J. K. Lee, *Biomacromolecules* **2011**, *12*, 625 – 632.
[16] H. S. Jung, K. J. Cho, Y. Seol, Y. Takagi, A. Dittmore, P. A. Roche, K. C. Neuman, *Adv. Funct. Mater.* **2018**, *28*, 1801252.
[17] S. Song, Y. Zhang, *J. Mater. Chem. A* **2017**, *5*, 22352 – 22360.
[18] T. Inokuchi, H. Kawafuchi, J. Nokami, *Chem. Commun.* **2005**, 537 – 539.
[19] D. Wang, L. Niu, Z. Qiao, D. Cheng, J. Wang, Y. Zhong, F. Bai, H. Wang, H. Fan, *ACS Nano* **2018**, *12*, 3796 – 3803.
[20] D. Cooper, N. Dimitrijevic, J. Nadeau, *Nanoscale* **2010**, *2*, 114 – 121.
[21] X. Wang, J. Zhang, Y. Wang, C. Wang, J. Xiao, Q. Zhang, Y. Cheng, *Biomaterials* **2016**, *81*, 114 – 124.
[22] M. Qin, X. Yang, K. Wang, X. Zhang, J. Song, M. Yao, D. Yan, B. Liu, Y. Zhao, *Nanoscale* **2015**, *7*, 19484 – 19492.
[23] X. Zhong, K. Yang, Z. Dong, X. Yi, Y. Wang, C. Ge, Y. Zhao, Z. Liu, *Adv. Funct. Mater.* **2015**, *25*, 7327 – 7336.

Manuscript received: February 28, 2019
Accepted manuscript online: April 10, 2019
Version of record online: May 21, 2019